

Derivation and application of new equations for radiation stress and volume flux

Baoxing Wang^{a,*}, Andrew J. Chadwick^a, Ashwini K. Otta^b

^a School of Engineering, University of Plymouth, PL4 8AA, United Kingdom

^b Samundra Institute of Maritime Studies, Lonavala, 410405, India

Received 5 February 2007; received in revised form 10 November 2007; accepted 23 November 2007

Available online 20 January 2008

Abstract

In this paper, new expressions of radiation stress and volume flux for long waves have been analytically derived by inclusion of higher-order surface elevations up to the sixth-order. To quantify these expressions, surface elevations along a beach are first simulated using the fully nonlinear Boussinesq-type model COULWAVE. Then, based on the large amount of numerical data, new equations for radiation stress and volume flux are statistically formulated. The research unveils the essential roles of the Ursell parameter, Irribarren number and wave steepness described by the local wave height, wave length and bottom slope. The study shows the importance of nonlinear wave properties in wave-induced currents and mean water levels (set-up/down). The higher-order formulations produce lower values for radiation stress and volume flux than calculated from the lower-order and linear waves. Case studies suggest that the new formulations produce an accurate estimation for mean water level. However, improvement on the computed current profiles is marginal for some cases. This implies that the accurate prediction of the current profile would require more than just the proposed improvement of the radiation stress and volume flux.

© 2007 Elsevier B.V. All rights reserved.

Keywords: Nonlinear waves; Radiation stress; Volume flux; Mean water levels; Currents

1. Introduction

Wave-induced currents and set-up/down (mean water level) strongly influence sediment transport process in the nearshore region. Significant progress has been made in the development of numerical models for nearshore circulation. Yet, our understanding of the nonlinear transformation of waves and currents is limited. The nonlinear effects induce significant changes in wave shape, height, length and phase velocity. Shoaling waves become more nonlinear; eventually the proximity of sea bottom will induce breaking and generate currents.

Wave-induced currents and set-up/down may be studied using either a time-dependent model or a time-averaged model with respect to the wave period. In recent years, the time-dependent (Boussinesq-type) models have reached a level of maturity. The governing equations behind some models, such as

COULWAVE (Lynett and Liu, 2004), allow for nonlinear transformation of waves over variable bathymetry to significant accuracy even for very high waves. One disadvantage of using such models is that they are computationally intensive, especially for simulation over a large area. Another disadvantage is that, an accurate formulation of an underlying current has not been achieved and the vertical profile of the currents cannot be predicted properly by such models.

The time-averaged models assume that the water motion may be split into a wave part and a current part. A recent advance in this respect is SHORECIRC model (Svendsen et al., Version 2.0), which is the three-dimensional modelling of wave-induced currents. Although the SHORECIRC model represents a major advance in the quasi-3D solution of the wave-induced circulation, two fundamental components (radiation stress and volume flux), have to be expressed in a linear way or corrected for nonlinear waves using weakly nonlinear wave theories and experimental formulations. Therefore, the main question facing the modeller now is how to represent wave nonlinearities when a time-averaged model is employed.

* Corresponding author. Fax: +44 1752233638.

E-mail address: baoxing.wang@plymouth.ac.uk (B. Wang).

In this study, the advantages of time-averaged mode and time-dependent model are combined. The improvements of formulation for radiation stress and volume flux are targeted. These formulations are derived analytically by inclusion of higher-order surface elevations. Our approach is to quantify the expressions using the data obtained from the model COUL-WAVE. The performances of the nonlinear formulations on setup and current profile are then demonstrated by their applications into the time-averaged model, e.g. the SHORECIRC model.

The organisation of the paper is as follows: Section 2 discusses the roles of radiation stress and volume flux in determining mean water level and currents. Section 3 presents the derivations of higher-order expressions of radiation stress and volume flux for long waves. The evolution of nonlinear waves on a beach then is studied using the Boussinesq-type model COULWAVE in Section 4. Statistical formulations of wave shape factor, shoaling coefficients and phase velocity are derived based on the numerical experiments. The performances of the new formulations are presented by comparisons to experimental data in Section 5. Finally, Section 6 summarises the conclusions.

2. Roles of radiation stress and volume flux in determining mean water level and currents

2.1. Governing equations

Current circulations over varying bottom topographies have been studied using two-dimensional horizontal (2-DH, depth-uniform currents) models, e.g. Ebersole and Dalrymple (1980) and Wu and Liu (1985). The models describe the depth-mean current and surface elevation and are based on depth-integrated and time-averaged Navier-stokes equations. By making the assumption of depth-uniform currents, the simplified equations were derived. However, the nearshore currents normally vary with the vertical location. The vertical variation is an important part of the mechanism that controls the horizontal distribution of circulation. Svendsen and Putrevu (1995) presented local solutions for the vertical structure of velocity profile both inside and outside the surf zone. They concluded that the local short-wave forcing cause a substantial vertical variations of current profiles where in the absence of such forcing the profiles are relatively depth-invariant. Van Dongeren and Svendsen (1997) presented the general quasi-3D expressions for horizontal momentums and continuity which can be solved numerically. The model based on this is now known as the SHORECIRC model. The time-averaged and depth-integrated equations of conservation of mass and momentum are derived for the general form of non-uniform currents over depth. After time-averaging, the short-wave motion is replaced by the radiation stress and the volume flux. The roles of radiation stress and volume flux are clearly demonstrated in the time-averaged equations. The detailed descriptions of the equations can be found in Svendsen et al. (Version 2.0). We outline the final forms of governing equation here.

2.1.1. Conservation of mass

$$\frac{\partial \bar{\zeta}}{\partial t} + \frac{\partial Q_\alpha}{\partial x_\alpha} = 0 \quad (2.1)$$

where $\bar{\zeta}$ represents the mean surface elevation. Q_α is the total volume flux, which is

$$Q_\alpha = \int_{-h_0}^{\bar{\zeta}} V_\alpha dz + \bar{Q}_{w\alpha} \quad (2.2)$$

where V_α is the current component. $\bar{Q}_{w\alpha}$ is the wave-induced volume flux and defined as a volume transport shoreward between crest and trough ζ_t of the wave, $\bar{Q}_{w\alpha} = \int_{\zeta_t}^{\bar{\zeta}} u_{w\alpha} dz \cdot u_{w\alpha}$ is the wave velocity.

2.1.2. Conservation of momentum

$$\begin{aligned} \frac{\partial Q_\beta}{\partial t} + \frac{\partial}{\partial x_\alpha} \left(\frac{Q_\alpha Q_\beta}{h} \right) + \frac{\partial}{\partial x_\alpha} \int_{-h_0}^{\bar{\zeta}} V_{d\alpha} V_{d\beta} dz \\ + \frac{\partial}{\partial x_\alpha} \int_{\zeta_t}^{\bar{\zeta}} (u_{w\alpha} V_{d\beta} + u_{w\beta} V_{d\alpha}) dz \\ = -g(h_0 + \bar{\zeta}) \frac{\partial \bar{\zeta}}{\partial x_\beta} - \frac{1}{\rho} \frac{\partial}{\partial x_\alpha} \\ \left[S'_{\alpha\beta} - \int_{-h_0}^{\bar{\zeta}} \tau_{\alpha\beta} dz \right] + \frac{\tau_{\beta}^S}{\rho} - \frac{\tau_{\beta}^B}{\rho} \end{aligned} \quad (2.3)$$

where ρ is the water density, p is the instantaneous pressure, g is gravitational acceleration, $V_{d\alpha}$ or $V_{d\beta}$ is depth-varying part, α and β represent the directions x and y in the Cartesian coordinate system, $\delta_{\alpha\beta}$ is the kronecker delta function and $\tau_{\alpha\beta}$ is turbulent (Reynolds) shear stress. τ_{β}^S and τ_{β}^B represent the surface and bottom shear stress respectively.

By including the currents, the radiation stress $S'_{\alpha\beta}$ is given as

$$S'_{\alpha\beta} = S_{\alpha\beta} - \rho \frac{Q_{w\alpha} Q_{w\beta}}{h} \quad (2.4)$$

$$S_{\alpha\beta} = \int_{-h_0}^{\bar{\zeta}} (p \delta_{\alpha\beta} + u_{w\alpha} u_{w\beta}) dz - \delta_{\alpha\beta} \frac{1}{2} \rho g (h_0 + \bar{\zeta})^2 \quad (2.5)$$

where $S_{\alpha\beta}$ is the radiation stresses defined as the excess flow of momentum due to the presence of waves only. $u_{w\alpha}$ and $u_{w\beta}$ are purely oscillatory part of wave velocity in α and β directions. h_0 is still water depth.

2.1.3. Currents profile

The effect of current distribution along the vertical was expressed semi-analytically. The total current component consists of three parts

$$V_\alpha = V_{m\alpha} + V_{dz}^{(0)} + V_{dz}^{(1)} \quad (2.6)$$

$V_{m\alpha}$ is the mean current, $V_{m\alpha} = Q_{\alpha w} / (h_0 + \bar{\zeta}) \cdot V_{d\alpha}^{(0)}$ is primarily the (slowly time varying) component created by local external forcing, the expression is given as

$$V_{d\alpha}^{(0)} = d_{1\alpha} \zeta^2 + e_{1\alpha} \zeta + f_{1\alpha} + f_{2\alpha} \quad (2.7)$$

where $\zeta = z + h_0$, $d_{1\alpha} = -\frac{F_{\alpha}}{2v_t}$, $e_{1\alpha} = \frac{\tau_{\alpha}^B}{\rho v_t}$, $f_{1\alpha} = -\frac{h}{2} \frac{\tau_{\alpha}^B}{\rho v_t}$, $f_{2\alpha} = \frac{h^2 F_{\alpha}}{6v_t}$, $F_{\alpha} = \left\{ \frac{1}{\rho h} \frac{\partial S'_{\alpha\beta}}{\partial x_{\beta}} + \frac{\tau_{\alpha}^B}{\rho h} - f_{\alpha} \right\}$, $f_{\alpha} = \frac{\partial}{\partial x_{\alpha}} (\overline{u_{w\alpha} u_{w\beta}}) + \frac{\partial}{\partial z} (\overline{u_{w\alpha} u_w})$.

The vertical variation of $V_{d\alpha}^{(1)}$ generated by the advective terms can be found in Svendsen et al. (Version 2.0).

It can be clearly seen that the radiation stress $S'_{\alpha\beta}$ or $S_{\alpha\beta}$ and the volume flux $Q_{w\alpha}$ play important roles in the variations of mean water level and current profile. The volume flux determines the magnitude of mean current $V_{m\alpha}$. The gradient of radiation stress $\frac{\partial S'_{\alpha\beta}}{\partial x}$ directly affects the gradient of mean water level $\frac{\partial \bar{\zeta}}{\partial x}$ and the component $V_{d\alpha}^{(0)}$ which is the primary current variation over water depth.

2.2. Existing expressions for radiation stress and volume flux

The concept of radiation stress developed in a series of publications by Longuet-Higgins and Stewart (1960, 1962, 1964) provided a fundamental theory to explain the mean water level variation outside and inside the surf zones. It comprises two components, i.e. the momentum part S_m and the pressure part S_p . In two horizontal dimensions, Svendsen et al. (Version 2.0) gave the generalised radiation stress tensor as

$$S_{\alpha\beta} = e_{\alpha\beta} S_m + \delta_{\alpha\beta} S_p \quad (2.8)$$

$$\text{with } e_{\alpha\beta} = \begin{bmatrix} \cos^2 \alpha_w & \cos \alpha_w \sin \alpha_w \\ \sin \alpha_w \cos \alpha_w & \sin^2 \alpha_w \end{bmatrix}.$$

For the linear wave theory, the momentum part is $S_m = \rho g H^2 (1 + G) / 16$ and the pressure part is $S_p = \rho g H^2 G / 16$, where $G = 2kh / \sinh 2kh$, k is wave number, h is local water depth, H is wave height. Without considering the roller, the volume flux of linear waves was given as in terms of wave height H and phase velocity c by Svendsen (2006), which is $Q_w = 0.125 g H^2 / c$.

To account for the wave nonlinearity, Svendsen (1984) used empirical information in terms of the dimensionless wave shape factor and roller area to represent the wave period-averaged properties. The wave shape factor is defined as $B_0 = \frac{1}{T} \int_0^T \left(\frac{\zeta}{H} \right)^2 dt = \frac{\bar{\zeta}^2}{H^2}$. The value of B_0 reflects the shape of the wave surface profile ζ . A sinusoidal wave has $B_0 = 0.125$. Svendsen and Putrevu (1993) concluded that results of the linear wave theory are far from satisfactory. Even the surf zone wave model given by Svendsen (1984) which empirically accounts for the actual shape of the waves described by B_0 is not quite satisfactory. The second order shape factor often has $B_0 \sim 0.04\text{--}0.05$ at the breaking point which is much smaller than a sinusoidal wave (Svendsen, 2006).

Waves propagating in shallow water, $kh < \pi/10$, are often called shallow water waves (Dean and Dalrymple, 1991). Based on shallow water wave theory, Svendsen (1984) assumed that the distribution of horizontal velocity is uniform from bottom to free surface. The horizontal velocity simply

equals to $u_0 = c\zeta/h$ and the wave phase velocity is $c = \sqrt{gh}$. Meanwhile the contribution from w^2 term (which represents the deviation from hydrostatic pressure) was neglected based on the assumption of $w^2 \ll u^2$. The time-averaged and depth-integrated volume flux and radiation stress are conventionally expressed in term of wave height H , wave shape factor B_0 , wave length L and phase velocity c . The mass flux and the radiation stress in two horizontal dimensions are expressed as

$$Q_{w\alpha} = \frac{gH^2}{c} \frac{c^2}{gh} \left[B_0 + \frac{A}{H^2} \frac{h}{L} \right] \frac{k_{\alpha}}{k} \quad (2.9)$$

$$S_{\alpha\beta} = e_{\alpha\beta} \rho g H^2 \frac{c^2}{gh} \left[B_0 + \frac{A}{H^2} \frac{h}{L} \right] + \delta_{\alpha\beta} \frac{1}{2} \rho g H^2 B_0 \quad (2.10)$$

where A is the roller area of the breaking wave in vertical projection.

In the shoaling zone, Svendsen et al. (2003) suggested that B_0 and c may be evaluated using the cnoidal wave theory. Hansen (1990) suggested the wave shape factor can be approximated by a simple function of Ursell number of cnoidal wave theory.

$$B_0 = 0.125 \tanh \left(11.40 / \sqrt{U} \right) \quad (2.11)$$

$$c = \sqrt{gh(1 + A_c H/h)} \text{ with } A_c = 1 - 0.0014 / \tanh \left(0.001 \sqrt{U} \right). \quad (2.12)$$

Hansen (1990) also used the experimental results to analyse a wide range of the wave shape factor in the surf zone. He proposed an empirical equation to estimate the factor B_0 inside the surf zone.

$$B_0 = B_{0B} [1 - a(b - h/h_B)(1 - h/h_B)] \quad (2.13)$$

in which B_{0B} is the value at the breaking point, and it can be determined with Eq. (2.11). h is the local water depth, h_B is the water depth at the breaking point. Coefficients a and b depend on deep water wave steepness and bottom slope. Their detailed expressions can be found in Hansen (1990).

Obviously, in addition to the phase speed and wave height, the wave shape factor B_0 is a parameter of fundamental importance in determining the radiation stress and volume flux. However, they are conventionally expressed by using either symmetric (about a vertical through the crest) profiles based on steady form solution (e.g. Cnoidal theory or Stream Function theory) or measured surface elevation from experiments. In the present paper, we seek formulations for wave shape factor, wave height and phase speed which incorporate the actual deformation of the waves as they propagate onshore. For this purpose, extended Boussinesq-type equations are sought. We will use the two-layer COULWAVE model whose one-layer version is identical to the formulation of Wei et al. (1995). The key feature of this set of Boussinesq-type equations is that it includes all nonlinear terms of higher-order consistent with the order of the (linear) dispersion equation. This was the remarkable departure from the earlier weakly nonlinear

Boussinesq-type equations which retained nonlinear terms only up to the first order. For certain benchmark cases, it has been shown by Wei et al. (1995) that the higher-order nonlinearity does improve the performance significantly and closely reproduce the transformation of high waves as predicted by the ‘exactly-non-linear’ boundary integral model. Further evidence of the improvement of the performance due to the higher-order nonlinear terms has been provided by Otta and Schäffer (1999) in the context of the steady permanent form waves. In a further extension, Lynett and Liu (2004) used two-layer approach to obtain a higher-order depth-integrated model. This two-layer model can be optimised to achieve a Pade’ [4/4] approximation of the exact linear relationship ($c^2/gh = \tanh(kh)/kh$) and it retains all the terms in the derivation consistently without the assumption of weak nonlinearity. Both the linear and nonlinear characteristics of this set are accurate up to $kh=6.5$.

3. Derivations of higher-order radiation stress and volume flux

As discussed in Section 2, the wave shape factor, which accounts for the second-order surface elevation, was widely used in the past to estimate the nonlinear wave properties. The derivation given by Svendsen (1984) was based on the assumption that the time-averaged higher-order surface elevation is negligible. However, it may not be true for fully nonlinear waves. By analysing the measurements by Ting and Kirby (1994), we found that the higher-order surface elevations are actually very significant. Svendsen and Staub (1981) also concluded that even if ζ^4/h^4 is included the error on depth-averaged velocity u_0 is up to 10% for $\zeta/h=0.6$. Therefore, the first-order expression $u_0=c\zeta/h$ can be regarded as a poor approximation. Very little is known of the higher-order effects on integrated wave properties so far. In this section, the task is to reformulate the radiation stress and volume flux by including the higher-order surface elevations. A basic premise of the present work is to investigate if the incorporation of the non-linear transformation in the calculation of the integrated wave properties becomes crucial for an accurate prediction of the set-up/down and currents.

Quantifications of radiation stress and volume flux for long waves require integration over time and depth of horizontal velocity. In a closed beach, the depth-integrated net flow must be zero. The depth-averaged velocity u_0 can be generally expressed in terms of the phase velocity c , the water depth h , the surface profile ζ and the height of surface roller in vertical projection e . The velocity profile used in the paper is illustrated in Fig. 1.

For the instantaneous balance of volume flux, one has

$$c\zeta = ce + u_0(h + \zeta - e) \tag{3.1}$$

$$u_0 = c \frac{\zeta - e}{h + \zeta - e} \tag{3.2}$$

where $h=h_0+\bar{\zeta}$, h_0 representing the still water level, $\bar{\zeta}$ denoting the mean water level.

Since it can be assumed that $\frac{e}{h+\zeta} \ll 1$ and $\frac{\zeta}{h} < 1$, Eq. (3.2) can be derived by Taylor series

$$u_0 = c \frac{\zeta - e}{h + \zeta - e} = c \frac{\zeta - e}{h + \zeta} \left(1 + \frac{e}{h + \zeta} - \left(\frac{e}{h + \zeta} \right)^2 + \dots \right) \approx c \frac{\zeta - e}{h + \zeta} = \frac{c\zeta}{h + \zeta} - \frac{ce}{h + \zeta} \tag{3.3}$$

$$u_0 = \frac{c}{h} \left(\zeta - \frac{\zeta^2}{h} + \frac{\zeta^3}{h^2} - \frac{\zeta^4}{h^3} + \frac{\zeta^5}{h^4} - \dots \right) - \frac{ce}{h} \left(1 - \frac{\zeta}{h} + \frac{\zeta^2}{h^2} - \frac{\zeta^3}{h^3} + \frac{\zeta^4}{h^4} - \frac{\zeta^5}{h^5} + \dots \right). \tag{3.4}$$

The time-averaged velocity \bar{u}_0 is given by

$$\bar{u}_0 = \frac{c}{h} \left(-\frac{\bar{\zeta}^2}{h} + \frac{\bar{\zeta}^3}{h^2} - \frac{\bar{\zeta}^4}{h^3} + \frac{\bar{\zeta}^5}{h^4} - \dots \right) - \frac{c\bar{e}}{h} \left(1 + \frac{\bar{\zeta}^2}{h^2} - \frac{\bar{\zeta}^3}{h^3} + \frac{\bar{\zeta}^4}{h^4} - \frac{\bar{\zeta}^5}{h^5} + \dots \right). \tag{3.5}$$

For \bar{e} , one has $\bar{e}=A/L$, where A is the area of the roller in vertical projection. L is the wave length. The purely oscillatory part of wave velocity $u_w = u_0 - \bar{u}_0$

$$u_w = \frac{c}{h} \left(\zeta - \frac{\zeta^2}{h} + \frac{\zeta^3}{h^2} - \frac{\zeta^4}{h^3} + \frac{\zeta^5}{h^4} - \dots \right) - \frac{ce}{h} \left(1 - \frac{\zeta}{h} + \frac{\zeta^2}{h^2} - \frac{\zeta^3}{h^3} + \frac{\zeta^4}{h^4} - \frac{\zeta^5}{h^5} + \dots \right) - \frac{c}{h} \left(-\frac{\bar{\zeta}^2}{h} + \frac{\bar{\zeta}^3}{h^2} - \frac{\bar{\zeta}^4}{h^3} + \frac{\bar{\zeta}^5}{h^4} - \dots \right) + \frac{c\bar{e}}{h} \left(1 + \frac{\bar{\zeta}^2}{h^2} - \frac{\bar{\zeta}^3}{h^3} + \frac{\bar{\zeta}^4}{h^4} - \frac{\bar{\zeta}^5}{h^5} + \dots \right) \tag{3.6}$$

3.1. Volume flux

$$Q_w = \int_{-h}^{\zeta} (u_0 - \bar{u}_0) dz + ce = \int_{-h}^{\zeta} u_0 dz - \int_{-h}^{\zeta} \bar{u}_0 dz + ce = u_0(\zeta + h) - \bar{u}_0(\zeta + h) + ce$$

$$\bar{Q}_w = \frac{u_0\bar{\zeta}}{\bar{\zeta}} + \bar{u}_0 h - \bar{u}_0(\bar{\zeta} + h) + ce = \frac{u_0\bar{\zeta}}{\bar{\zeta}} + c\bar{e} \text{ with the assumption } \bar{\zeta} \approx 0$$

$$u_0\bar{\zeta} = \frac{c}{h} \left(\zeta^2 - \frac{\zeta^3}{h} + \frac{\zeta^4}{h^2} - \frac{\zeta^5}{h^3} + \frac{\zeta^6}{h^4} - \dots \right) - \frac{ce}{h} \left(\zeta - \frac{\zeta^2}{h} + \frac{\zeta^3}{h^2} - \frac{\zeta^4}{h^3} + \frac{\zeta^5}{h^4} - \frac{\zeta^6}{h^5} + \dots \right)$$

$$\bar{u}_0\bar{\zeta} = \frac{c}{h} \left(\bar{\zeta}^2 - \frac{\bar{\zeta}^3}{h} + \frac{\bar{\zeta}^4}{h^2} - \frac{\bar{\zeta}^5}{h^3} + \frac{\bar{\zeta}^6}{h^4} - \dots \right) - \frac{c\bar{e}}{h} \left(\bar{\zeta} - \frac{\bar{\zeta}^2}{h} + \frac{\bar{\zeta}^3}{h^2} - \frac{\bar{\zeta}^4}{h^3} + \frac{\bar{\zeta}^5}{h^4} - \frac{\bar{\zeta}^6}{h^5} + \dots \right)$$

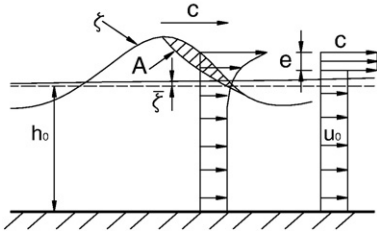


Fig. 1. Sketch of velocity profile.

Due to the small value of \bar{e} , term $\frac{c\bar{e}}{h} \left(\bar{\zeta} - \frac{\bar{\zeta}^2}{h} + \frac{\bar{\zeta}^3}{h^2} - \frac{\bar{\zeta}^4}{h^3} + \frac{\bar{\zeta}^5}{h^4} - \frac{\bar{\zeta}^6}{h^5} + \dots \right)$ may be neglected. Therefore, one has

$$\bar{Q}_w = \frac{gH^2 c^2}{c gh} \left\{ \left(\frac{\bar{\zeta}^2}{H^2} - \gamma \frac{\bar{\zeta}^3}{H^2} + \gamma^2 \frac{\bar{\zeta}^4}{H^2} - \gamma^3 \frac{\bar{\zeta}^5}{H^2} + \gamma^4 \frac{\bar{\zeta}^6}{H^2} - \dots \right) + \frac{h A}{L H^2} \right\} \quad (3.7)$$

where $\gamma = H/h$.

3.2. Radiation stress

By neglecting the contribution of vertical velocity w , the expression for radiation stress in the wave propagation direction is

$$\begin{aligned} S &\approx \int_{-h}^{\zeta} \overline{\rho u_w^2} dz + \frac{1}{2} \rho g \bar{\zeta}^2 + \rho \frac{A}{L} c^2 \\ &= \int_{-h}^0 \overline{\rho u_w^2} dz + \int_0^{\zeta} \overline{\rho u_w^2} dz + \frac{1}{2} \rho g \bar{\zeta}^2 + \rho \frac{A}{L} c^2 \end{aligned} \quad (3.8)$$

$$u_w^2 = (u_0 - \bar{u}_0)^2. \quad (3.9)$$

Neglecting the higher-order term $(\bar{e}/h)^2$ and the interactions between e (or \bar{e}) and higher-order surface elevations, one obtains

$$\int_0^{\zeta} \overline{\rho u_w^2} dz = \rho g \frac{c^2}{gh} \left[\frac{\bar{\zeta}^3}{h} - \frac{2}{h^2} \bar{\zeta}^4 + \frac{3}{h^3} \bar{\zeta}^5 - \frac{4}{h^4} \bar{\zeta}^6 + \dots \right] \quad (3.10)$$

$$\int_{-h}^0 \overline{u_w^2} dz = \rho g \frac{c^2}{gh} \left(\bar{\zeta}^2 - 2 \frac{\bar{\zeta}^3}{h} + \frac{3}{h^2} \bar{\zeta}^4 - \frac{4}{h^3} \bar{\zeta}^5 + \frac{5}{h^4} \bar{\zeta}^6 + \dots \right) \quad (3.11)$$

$$S = \rho g H^2 \left[\frac{c^2}{gh} \left(B_2 - \gamma \frac{\bar{\zeta}^3}{H^3} + \gamma^2 \frac{\bar{\zeta}^4}{H^4} - \gamma^3 \frac{\bar{\zeta}^5}{H^5} + \gamma^4 \frac{\bar{\zeta}^6}{H^6} - \dots \right) + \frac{1}{2} B_2 + \frac{c^2 A h}{gh H^2 L} \right] \quad (3.12)$$

where $B_2 = \bar{\zeta}^2/H^2$, $\gamma = H/h$.

To distinguish the higher-order formulation from the previous Eqs. (2.9) and (2.10), the wave shape factor, volume flux and radiation stress are redefined as

The second-order expression:

$$B_2 = \frac{\bar{\zeta}^2}{H^2} \quad (3.13)$$

$$Q_{wz} = \frac{gH^2 c^2}{c gh} \left[B_2 + \frac{A h}{H^2 L} \right] \frac{k_x}{k} \quad (3.14)$$

$$s_{\alpha\beta} = e_{\alpha\beta} \rho g H^2 \frac{c^2}{gh} \left[B_2 + \frac{A h}{H^2 L} \right] + \delta_{\alpha\beta} \frac{1}{2} \rho g H^2 B_2. \quad (3.15)$$

The sixth-order expression:

$$B_6 = \frac{\bar{\zeta}^2}{H^2} - \gamma \frac{\bar{\zeta}^3}{H^3} + \gamma^2 \frac{\bar{\zeta}^4}{H^4} - \gamma^3 \frac{\bar{\zeta}^5}{H^5} + \gamma^4 \frac{\bar{\zeta}^6}{H^6} \quad (3.16)$$

$$Q_{zw} = \frac{gH^2 c^2}{c gh} \left[B_6 + \frac{A h}{H^2 L} \right] \frac{k_x}{k} \quad (3.17)$$

$$S_{\alpha\beta} = e_{\alpha\beta} \rho g H^2 \frac{c^2}{gh} \left[B_6 + \frac{A h}{H^2 L} \right] + \delta_{\alpha\beta} \frac{1}{2} \rho g H^2 B_2. \quad (3.18)$$

We can see that, except the first term in shape factor, the contributions of time-averaged higher-order surface elevations to shape factor are modified by the ratio of wave height to water depth $\gamma = H/h$. It means that the effects of high order terms will disappear in intermediate or deep water $H/h \rightarrow 0$. Moreover, a positive contribution is made by the surface elevation with an even exponent and an odd exponent makes a negative contribution.

The higher-order surface elevations may be related to widely used time series parameters, such as the standard deviation of water surface σ , the third central moment (skewness) $S_\zeta = \sum \zeta^3 / (\sigma^3 N)$ and the fourth central moment (kurtosis) $K_\zeta = \sum \zeta^4 / (\sigma^4 N)$, where N is the number of sample. The relations may be established as $\bar{\zeta}^2/H^2 = \sigma^2/H^2$, $\bar{\zeta}^3/H^3 = S_\zeta \sigma^3/H^3$ and $\bar{\zeta}^4/H^4 = K_\zeta \sigma^4/H^4$.

Skewness is an important indicator of nonlinear wave behaviour and a measure of the vertical asymmetry. When wave crest heights are larger than the trough depths, as is the case for shallow water waves, the skewness has a positive value. Positively skewed waves present a smaller shape factor. Wave kurtosis represents a degree of the peakedness. Based on its definition, kurtosis will make a positive contribution to the wave shape factor, and balance in part the negative effects by skewness.

Having derived the higher-order radiation stress and volume flux, we need to quantify the expressions for practical application. The investigation and formulations will be carried out in Section 4.

4. The Boussinesq model simulations

4.1. Description of the numerical flume

The Boussinesq-type model, COULWAVE, developed by Lynett and Liu (2004) has been employed to investigate the

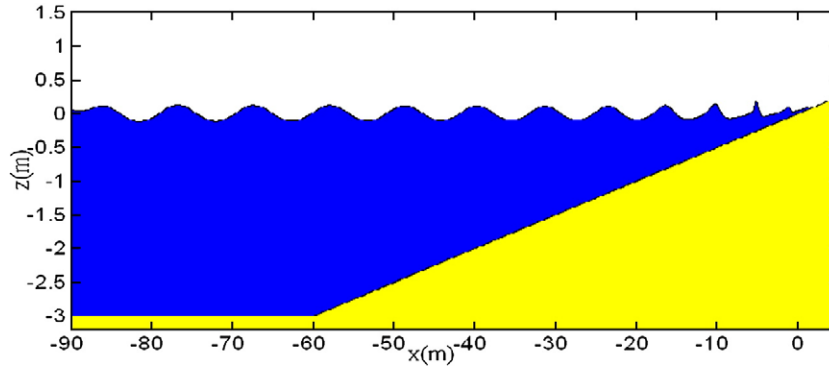


Fig. 2. Sketch of numerical flume.

nonlinear long-period wave properties over a simple bathymetry profile. The model allows for the evolution of fully nonlinear waves over variable bathymetry, which implies wave amplitude/water depth = $O(1)$. Our investigation is limited to monochromatic waves shoaling and breaking in a direction normal to the shoreline. A typical domain of the simulation is sketched in Fig. 2. A wavemaker is specified on the leftward boundary in the numerical flume. The length of flat portion is 30 m and the water depth is 3.0 m.

A parametric study for various environmental conditions is carried out to assess the nonlinear effects. To accurately predict nonlinear wave properties, it will be shown that, in addition to

incident wave conditions (wave height and period), the beach slope must be taken into account. The inclusion of these physical processes is essential to improve quantitative understanding of the nonlinear wave properties. Beach slopes are set as 1/50, 1/40, 1/35, 1/30, 1/25 and 1/20. Preliminary results of simulations indicates instability may occur for steeper slopes ($>1/20$) at the shoreline boundary. Therefore, the investigation of the slopes steeper than 1/20 is not further attempted. For those slopes smaller than 1/50 require a tremendous amount of computer memory and CPU time, and have not been included in the research.

Although incident waves can be arbitrary in the numerical model, for the sake of comparison with the experiments carried

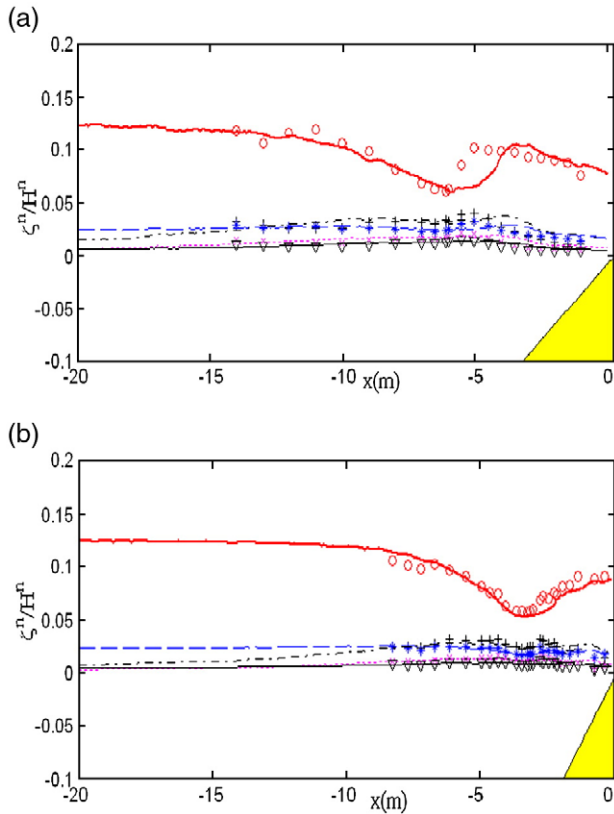


Fig. 3. Time-averaged surface elevations for Case 1 (a) and Case 3 (b). Simulations: ζ^2/H^2 (wide solid line), ζ^3/H^3 (dash-dotted line), ζ^4/H^4 (dash line), ζ^5/H^5 (dotted line), ζ^6/H^6 (solid line). Observations: ζ^2/H^2 (o), ζ^3/H^3 (+), ζ^4/H^4 (*), ζ^5/H^5 (x), ζ^6/H^6 (∇).

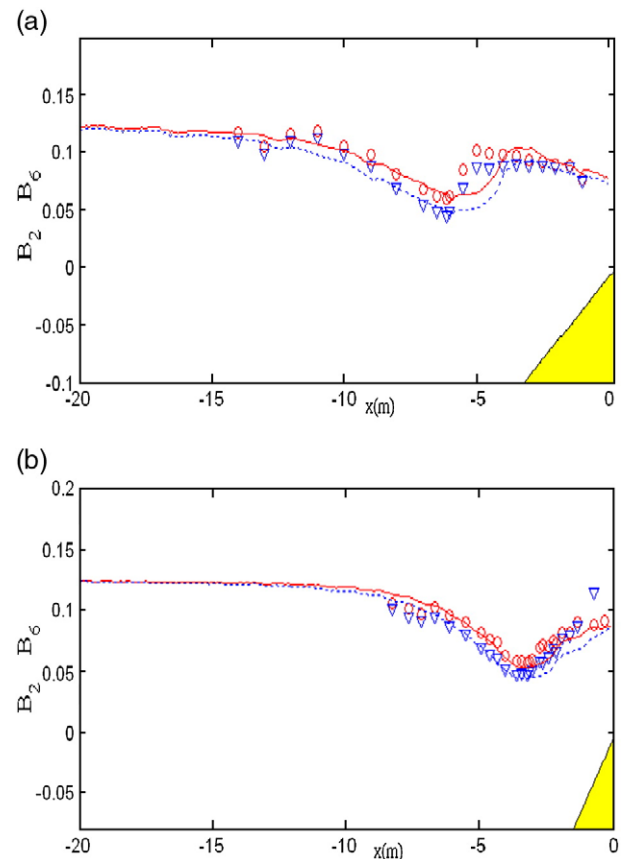


Fig. 4. Shape factors for Case 1 (a) and Case 3 (b). Observations: B_2 (o), B_6 (∇), Simulations: B_2 (solid line), B_6 (dotted line).

in the laboratories, four different wave periods $T=2.0$ s, 2.5 s, 4.0 s, and 5.0 s are used in the research. Combined with these wave periods, a large range of incident wave heights is specified at the upstream boundary of the computational domain. Sinusoidal waves with incoming wave height equal to 0.04 m, 0.05 m, 0.065 m, 0.08 m, 0.10 m, 0.15 m, 0.20 m and 0.25 m, are propagated from the left to the right. The wave heights and periods are chosen based on the generation of quasi-steady sine waves and a more uniform spread of nonlinear wave parameters, such as the Ursell number and wave steepness in the shoaling and breaking zones. The values of kh vary from 0.76 to 3.01 which are in the range of COULWAVE model capability. Each wave height is combined with four wave periods and six beach slopes. The total combinations of simulation cases are 159. Note that a large amount of data is of fundamental importance to statistically formulate the nonlinear wave properties. The incident wave conditions are also inspected against the possible breaker types. For the present wave inputs, the maximum and minimum values of offshore Iribarren numbers are 1.53 and 0.10. Surging and collapsing breakers are not included, and the breaker types are either spilling or plunging.

4.2. Scope of investigation

Our study is concentrated on the simulation of wave surface elevation and phase velocity. Time series of surface elevations were generated at selected grid points along the numerical wave flume. The duration of each realization is about 40 s. The simulations indicate that quasi-steady conditions have reached within 40 s, even for those long waves. Further increasing the length of the realization does not have any impact of output. Using the time series of surface elevation, the averaged wave crest, trough, height H , and high order surface elevations $\bar{\zeta}^2/H^2$, $\bar{\zeta}^3/H^3$, $\bar{\zeta}^4/H^4$, $\bar{\zeta}^5/H^5$ and $\bar{\zeta}^6/H^6$ are calculated over eight to fifteen successive waves.

The recorded surface elevations are also used to estimate wave phase velocity. The numerical wave gages are specified at fixed locations along the beach. Each crest and trough of the propagating waves are identified and followed in space and time from the generation at the upstream boundary to the shoreline. The local phase velocity can be obtained as $c(x)=\Delta x/\Delta t$, where Δx denotes the distance between two successive crest (or trough) locations of the snapshots, and Δt is time interval between snapshots. The numerically observed phase velocities oscillate along the flume due to the reflection from the beach and the broken waves. With the aid of nonlinear least square regression, one can eliminate these fluctuations to determine the phase velocity. The nonlinearly smoothed phase velocity will be used to estimate the local wave length $L(x)=c(x)T$, where T is wave period.

With wave height H , length L , local water depth h and beach slope, the Iribarren number, Ursell number and wave steepness can be obtained. It is expected that the expressions for wave shape factor and phase velocity can be characterized by these parameters, and their formulations may be derived statistically from the simulated data sets.

4.3. Model performances

The performances of COULWAVE model have been well presented in Lynett (2006) in terms of wave surface elevations. As shown in Section 3, the wave shape factors are expressed in time-averaged surface elevations scaled by wave height ($\bar{\zeta}^n/H^n$, $2 \leq n \leq 6$). In recognizing the importance of $\bar{\zeta}^n/H^n$ for the shape factors, the comparisons between measured and simulated results are demonstrated here.

Four sets of physical experiments for regular waves are selected and examined. These data sets are referred to as *Case 1* with $T=2.0$ s and slope=1/35 (Ting and Kirby, 1994, 1995, 1996), *Case 2* with $T=5.0$ s and slope=1/35 (Ting and Kirby, 1994, 1995, 1996), *Case 3* with $T=2.5$ s, slope=1/20 (Govender et al., 2002), *Case 4* with $T=4.0$ s, slope=1/20 (De Serio and Mossa, 2006). The detailed descriptions of experiment set-up can be found in their published papers.

The simulated data for all four cases present a good correlation with the measurements. Fig. 3 displays the results for Case 1 and Case 3. We can see that the second-order term $\bar{\zeta}^2/H^2$ is 0.125 in deep water, and decreases to a minimum value near the breaking point. As expected, the third-order term (proportional to the skewness) is nil for a sine wave in deep water and gradually increases as waves propagate from offshore to the nearshore. The trend of fourth order of $\bar{\zeta}^4/H^4$ is similar to the second order. Compared with $\bar{\zeta}^2/H^2$, the higher-order values $\bar{\zeta}^3/H^3$ and $\bar{\zeta}^4/H^4$ are significant, particularly in shallow water. For instance, the ratio of $\bar{\zeta}^3/H^3$ to $\bar{\zeta}^2/H^2$ can reach 0.50 for the wave conditions tested.

As shown in Fig. 3, the model also demonstrates its ability to predict the higher-order terms. The simulations of $\bar{\zeta}^5/H^5$ and $\bar{\zeta}^6/H^6$ are in good agreement with experimental data in terms of magnitude and trend. The comparisons provide sufficient base to use these higher-order terms up to the sixth in present investigation. Comparing to those lower-order terms, much smaller values of $\bar{\zeta}^5/H^5$ and $\bar{\zeta}^6/H^6$ are present. It indicates less importance of higher-order surface elevations after the fourth order.

Having known the values of $\bar{\zeta}^n/H^n$, we can compute the shape factors, B_2 and B_6 . It is worthwhile mentioning here that shape factors converge quickly in response to $\bar{\zeta}^n/H^n$. The analysis indicates that the difference between the sixth-order and the eighth-order is about 1%. Therefore, inclusion of the sixth-order is sufficient to obtain a reasonable accuracy.

The comparisons of shape factor are made in Fig. 4 for Case 1 and Case 3 respectively. The nonlinear shape factor is radically different from the simplified sinusoidal value. B_2 and B_6 have a same value of 0.125 at deep water but diverge from each other in shallow water. The higher-order shape factor B_6 presents a lower value than B_2 .

4.4. Phase velocity

Using some conventional finite-amplitude wave theories, e.g. cnoidal wave theory and the stream function theory, the nonlinear wave phase velocity may be calculated numerically. However, neither of them can be applied in the region near the breaking point. In our investigation, the phase velocity is

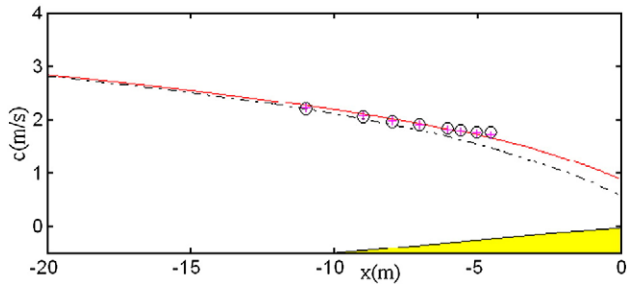


Fig. 5. Phase velocity for Case 3. Simulated (solid line), linear wave (dash-dotted line), cnoidal wave (o) and stream function (+).

estimated using the method described in Section 4.2. It is expected that the approach will approximate the nonlinear wave phase to some extent.

The numerical results from the COULWAVE model are compared with those based on the linear, cnoidal and stream function theories. One example of the comparisons is given in Fig. 5. The linear wave theory produces the smallest wave phase velocity due to the assumption of small-amplitude. The simulations suggest that, in intermediate and deep water, the wave phase velocity estimated by the model reasonably approaches the results computed by linear wave theory. The results from cnoidal and stream function theories are situated around the COULWAVE numerical experiments. This confirms the finite amplitude effects from the Boussinesq dispersion relation. Although our approach used here may not be a precise method, it gives a reasonable approximation of the nonlinear wave phase velocity.

4.5. Simulation results and formulations

The COULWAVE model has demonstrated its efficiency to study wave transformation under various scenarios. Having tested its performances, its use in the investigation is straightforward although computations are intensive. The grouped results for $T=5$ s, $H=0.04$ m, 0.05 m, 0.065 m, 0.08 m, 0.10 m, 0.15 m, 0.20 m, 0.25 m, slope=1/50, present some features common to other groups, and are discussed here.

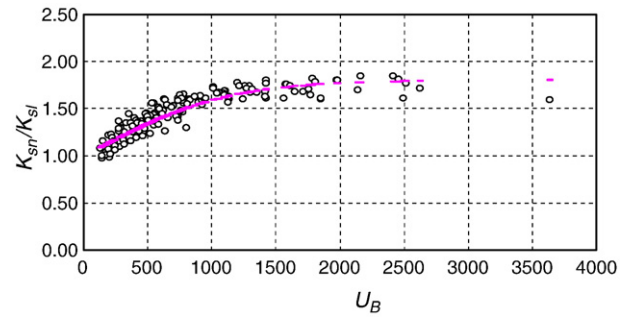


Fig. 7. K_{sn}/K_{sl} versus U_B at breaking point. Observations (o), predictions (-).

4.5.1. Analysis of shoaling coefficient

The shoaling coefficient is defined as $K_{sl}=H/H_o$, where H is the local wave height and H_o is the wave height in deep water. The shoaling coefficient from the linear wave theory can be calculated by Eq. (3.16) in Goda (2000). As waves approach very shallow water, shoaling becomes highly nonlinear. The linear shoaling coefficient significantly under predicts the wave height. Nonlinear shoaling coefficients are available in several publications (Goda, 2000; SPM, 1984), in which the shoaling coefficients are related to parameters of wave steepness, relative depth and beach slopes.

In the present study, the shoaling coefficients are investigated using the numerical results from the fully nonlinear COULWAVE model. Both the linear shoaling coefficients K_{sl} and the nonlinear shoaling coefficients K_{sn} are computed up to the breaking point. As shown in Fig. 6, the ratios between K_{sn} and K_{sl} demonstrate a strong connection to the local Ursell numbers along a beach. Fig. 7 shows the relation between K_{sn} and K_{sl} at the various breaking points for different cases. Both Figs. 6 and 7 suggest that the nonlinear effects on the shoaling coefficient depend on the local Ursell numbers. When Ursell number is low, the observed shoaling coefficients agree with the those from the linear theory $K_{sn}/K_{sl} \rightarrow 1.0$. The nonlinear influences become larger as Ursell numbers increase up to around $U=1500$. The maximum value of K_{sn}/K_{sl} can reach 1.8. A further increase in Ursell number will not produce more

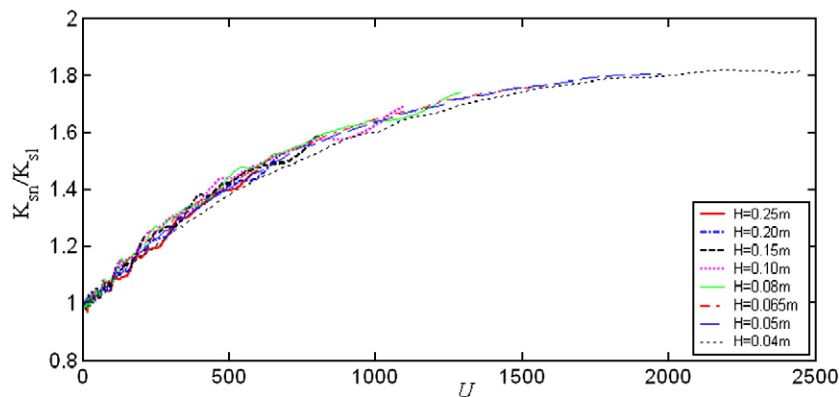


Fig. 6. K_{sn}/K_{sl} versus Ursell parameters along a beach.

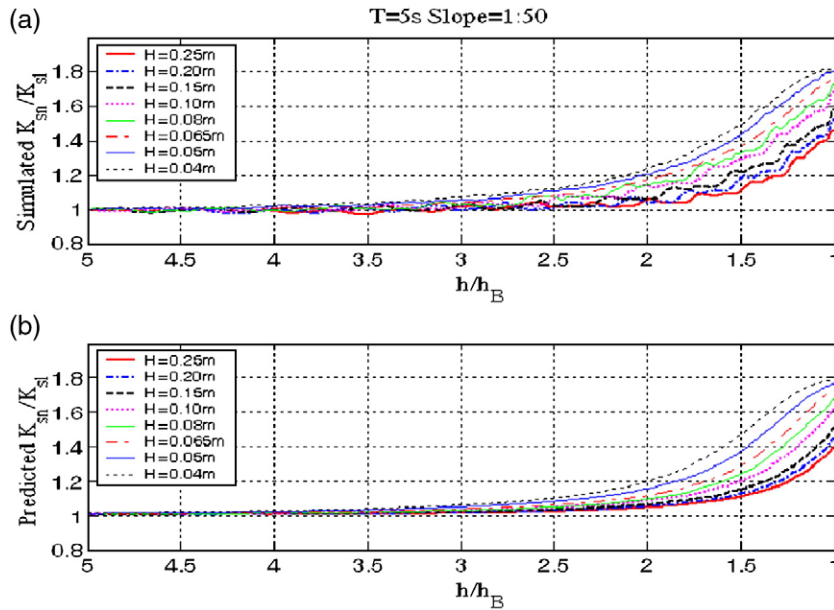


Fig. 8. K_{sn}/K_{sl} versus h/h_B , (a) observations, (b) predictions.

impact on the shoaling coefficients. It has been found here that the relation may be approximated as:

$$K_{sn}/K_{sl} = 1 + 0.80 \tanh(U/1070)^{1.06}. \quad (4.1)$$

The performance of Eq. (4.1) is displayed in Fig. 8. The predicted shoaling amplification of wave height is in reasonable agreement with the numerical observations.

4.5.2. Wave shape factors

Figs. 9 and 10 show the variations of B_2 and B_6 in the group versus the dimensionless water depth h/h_B . The waves begin with a nearly sinusoidal shape factor of 0.125 in deep or intermediate water, and then are transformed to a spilling breaker or plunging breaker with a significantly reduced shape factor. At the breaking point, the wave shape factors present the lowest value, and the shape factor can be as low as 0.025 (B_2) and 0.23 (B_6), much smaller than for a sinusoidal wave. B_2 and B_6

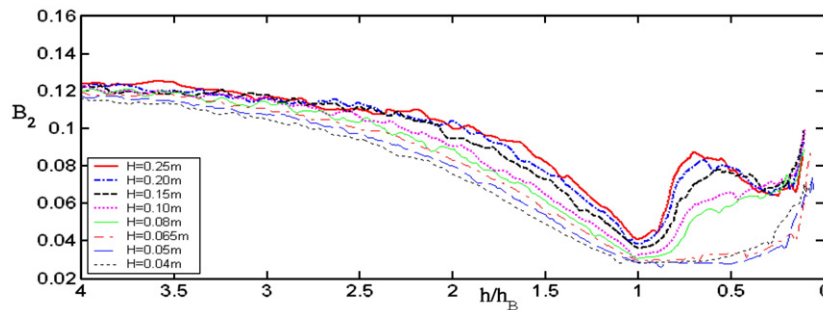


Fig. 9. Variations of B_2 against relative water depth h/h_B .

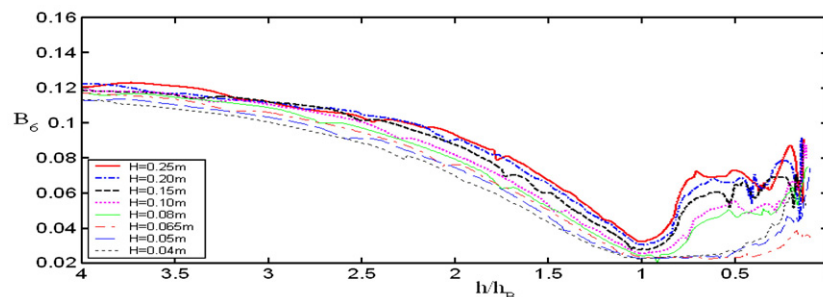


Fig. 10. Variations of B_6 against relative water depth h/h_B .

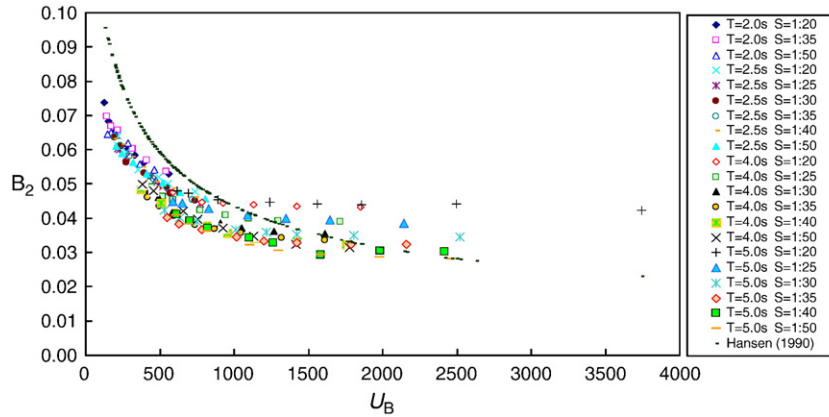


Fig. 11. B_2 versus Ursell number U_B at breaking point.

exhibit the same variation trend, but differ in their magnitudes. For all simulated cases, B_2 is 5–23% bigger than B_6 at the breaking point.

After initiation of breaking, waves regain some symmetry accompanied by a rapid decay in height. For a spilling breaker, the wave shape factor increases to a maximum value and thereafter decrease again toward the shoreline, but it seems that it does not reach the same low value as at breaking. For a plunging breaker, the wave shape factor continually increases in the surf zone, but will be always less than 0.125. Due to the different trends of variation, the shape factors in shoaling and surf zones will be formulated separately.

4.5.2.1. B_2 and B_6 in the shoaling zone. The Ursell number U is a traditional parameter expressing the balance between shallow-water steepening and the effect of water acceleration (Peregrine, 1983). The role as rated by the Ursell number can increase from a small value in deep water to a large value in near-shore shallow water. This indicates that the effects of nonlinearity (amplitude dispersion) gradually become important. Figs. 11 and 12 illustrate the shape factors B_2 and B_6 versus Ursell number U_B at breaking point. Two important features can be identified from the figures. Indeed, the local Ursell numbers have a crucial influence on the shape factors. As the Ursell numbers increase, the shape factors are reduced. The

decrease of shape factor becomes slow when the Ursell number is larger than 1500.

The interpretation of wave shape factor corresponding only to the local Ursell number is inadequate. The variation trends of wave shape factor diverge as the Ursell numbers increase. It is found that another important parameter, the Irribarren number plays an important role in determining shape factors as well. Under the same Ursell numbers, the relations between B_6 and the Irribarren number ξ_B at the breaking point are shown in Fig. 13. It can be clearly seen that the shape factors tend to increase as the Irribarren numbers increase.

According to the definition of Irribarren number $\xi = \tan \alpha / (H/L)^{1/2}$, it actually represents the influences of the beach slope and the wave steepness. Under the same Ursell number, the shoaling evolution may be much stronger on a gentle slope than on a steep slope. We may also see that the dependence on the Irribarren number is more evident for those large Ursell numbers.

Based on the simulated data sets, the nonlinear regression analysis has been undertaken to determine the coefficients of the local parameters (Ursell number U and Irribarren number ξ) that cause a function to best fit our observations. Hansen (1990) suggested that the shape factors depend on the Ursell number U through a hyperbolic tangent function, see Eq. (2.11) as shown in Fig. 11. The similar function is used here but modified by an exponential function of the Irribarren number.

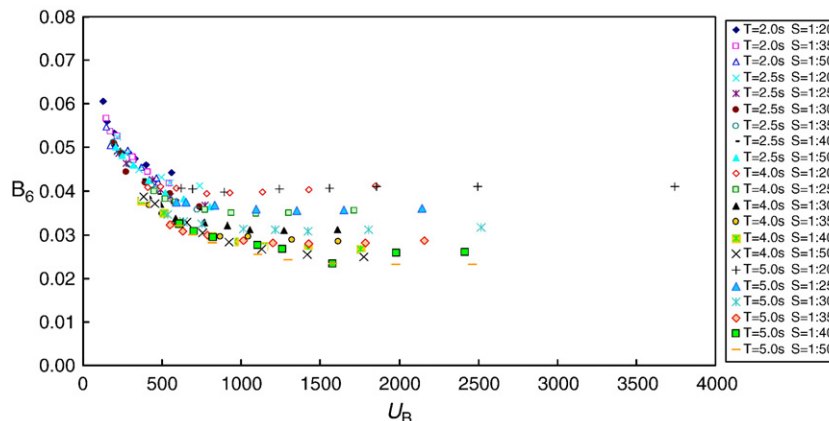


Fig. 12. B_6 versus Ursell number U_B at breaking point.

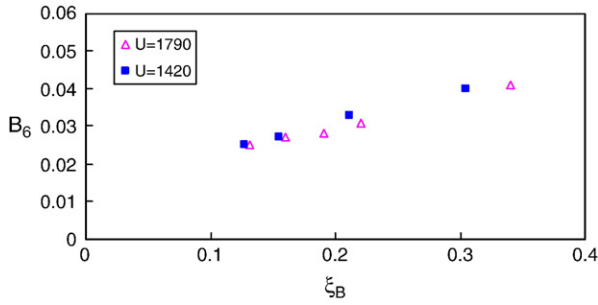


Fig. 13. B_6 versus Iribarren number ξ_B at breaking point.

Owing to the importance of prediction at the breaking point, the expressions at the breaking point are sought first. The analysis leads two expressions for B_2 and B_6 at the breaking point respectively.

$$B_2 = 0.125 \tanh(3.82U^{-0.38} e^{5\xi^2}) \quad (4.2)$$

$$B_6 = 0.125 \tanh(2.34U^{-0.35} e^{6\xi^2}). \quad (4.3)$$

Before the breaking point, the expressions for shape factor are obtained by multiplying the relative water depth, which give

$$B_2 = 0.125 \tanh(3.82(h/h_B)^{0.30} U^{-0.38} e^{5\xi^2}) \quad (4.4)$$

$$B_6 = 0.125 \tanh[2.34(h/h_B)^{0.50} U^{-0.35} e^{6\xi^2}]. \quad (4.5)$$

The predicted and the observations at the breaking point are linearly well related. The correlation coefficients are $R^2=0.90$ for B_2 and $R^2=0.88$ for B_6 .

4.5.2.2. B_2 and B_6 in the surf zone. The shape factors in the surf zone exhibit a very complex pattern. Hansen (1990) noted

that variation of B_2 with deep water steepness H_o/L_o and beach slope. It is found here that shape factors are controlled by their local wave steepness H/L , shape factor at breaking point B_{2B} or B_{6B} and the location in the surf zone h/h_B . The individual role of the parameters involved is examined by the comparisons between the variation trends of shape factor and the parametric wave inputs. The expressions are formulated as Eqs. (4.6) and (4.7). The role of each term is discussed in what follows.

$$B_2 = B_{2B} \{ 1 + 2 \tanh(5\alpha_B \varphi) \exp[-40\alpha_B^2 \chi_B (1 - h/h_B)] \} \quad (4.6)$$

$$B_6 = B_{6B} \{ 1 + 2.5 \tanh(5\alpha_B \varphi) \exp[-40\alpha_B^2 \chi_B (1 - h/h_B)] \} \quad (4.7)$$

where $\alpha_B = B_{2B}/0.125$ for B_2 and $\alpha_B = B_{6B}/0.125$ for B_6 . $\varphi = \chi_B/\chi - 1$, $\chi = \sqrt{H/L}$, $\chi_B = \sqrt{H_B/L_B}$.

Wave shoaling processes cause waves to steepen, with short steep crests and broad shallow troughs. When wave slopes at the crest become sufficiently steep, the waves break. Following the initiation of breaking, wave shapes reform and their steepness decreases. The steepness variation is described here by the parameter $\varphi = \chi_B/\chi - 1$. It is observed that for a spilling breaker, the shape factor quickly increases to a maximum value in a short distance, while a plunging breaker regains its shape in nearly the entire surf zone. Therefore, the bigger an initial shape factor at the breaking point, the quicker an increase in shape factor after breaking. This implies that the dimensionless parameter $\alpha_B = B_B/0.125$ affects the development of wave shape. The data analysis found that the variation trend can be represented by the function of $\tanh(5\alpha_B \varphi)$. The coefficient of five in the function was obtained by nonlinear least square fitting.

A spilling breaker quickly increases its shape factor to a maximum value and then decreases again toward the shoreline.

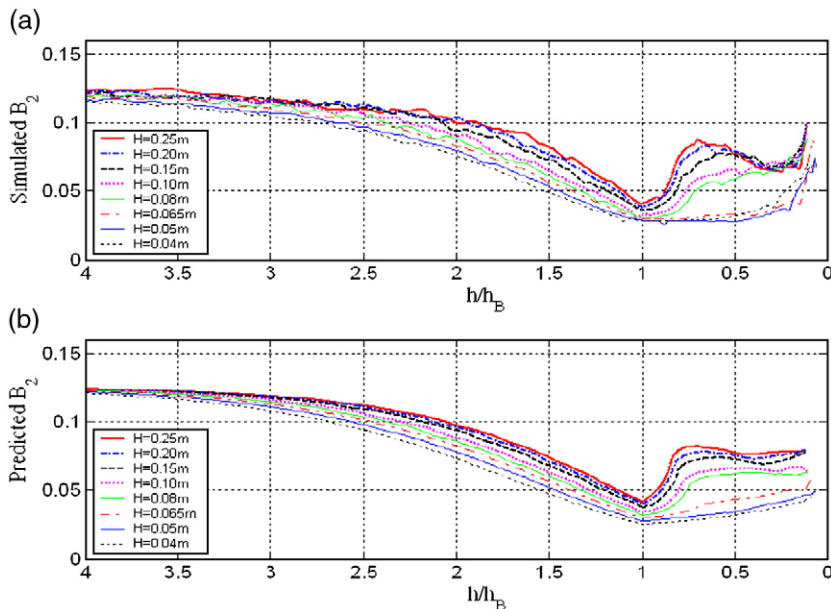


Fig. 14. Comparisons between (a) the numerical simulations and (b) the analytical predictions for B_2 .

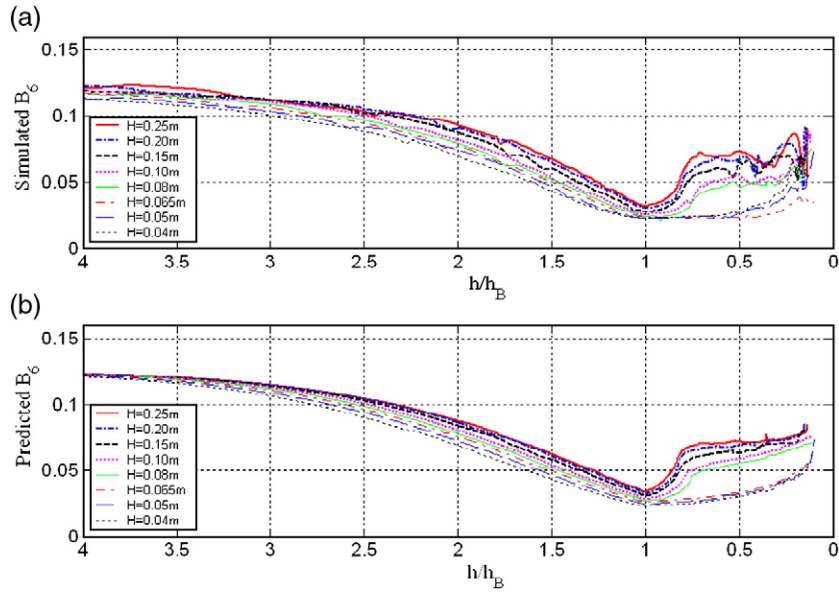


Fig. 15. Comparisons between the numerical simulations (a) and analytical predictions (b) for B_6 .

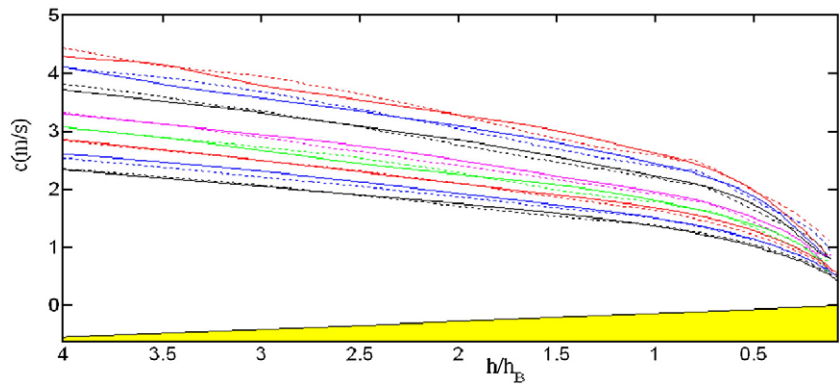


Fig. 16. Numerical and analytical wave phase velocities. Analytical solutions (dashed line), Numerical simulations (solid line).

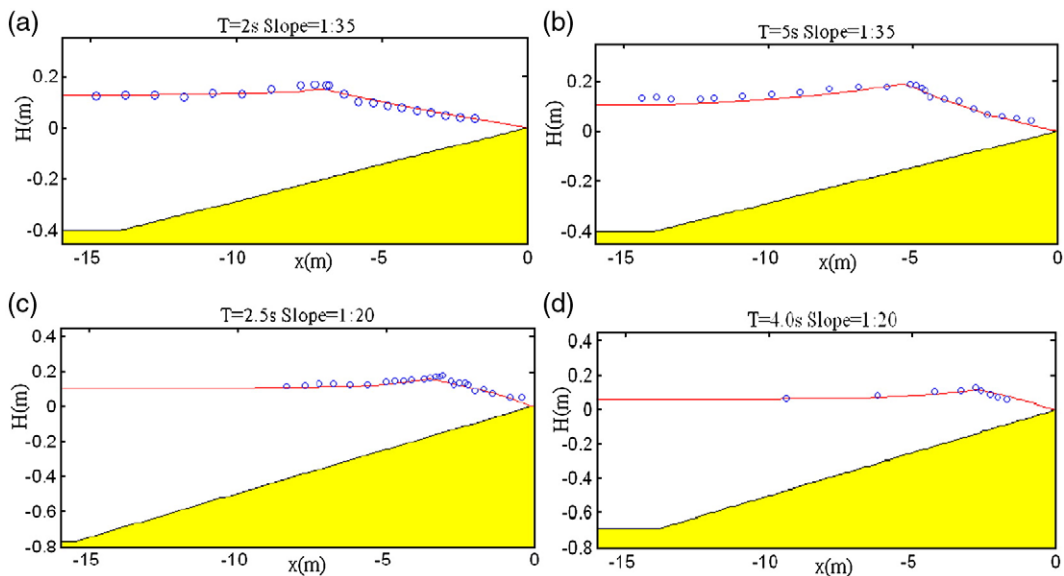


Fig. 17. Wave heights for Case 1 (a), Case 2 (b), Case 3 (c) and Case 4 (d). Measurements (o), predictions (solid line).

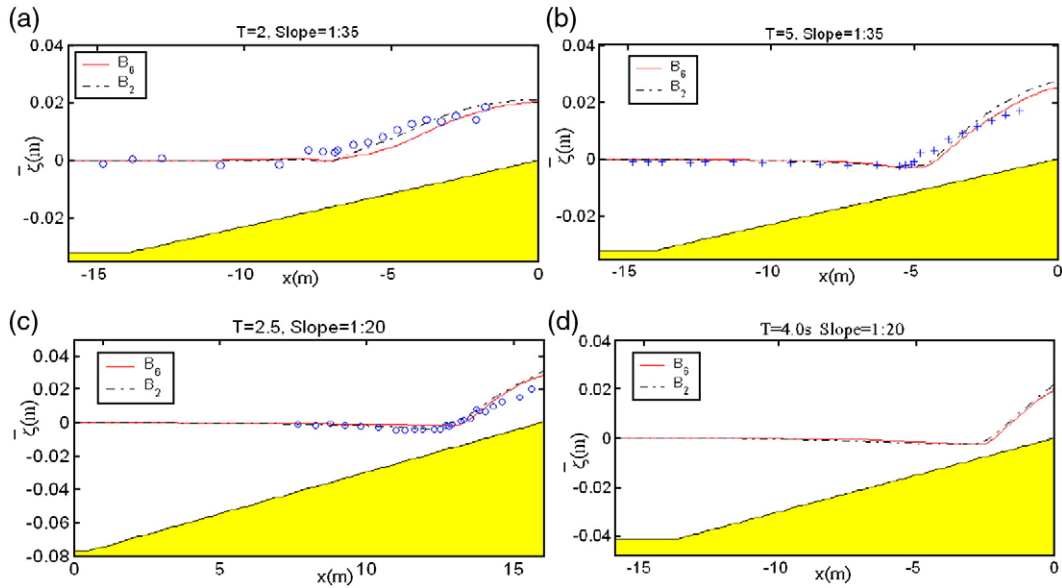


Fig. 18. Mean water levels for Case 1 (a), Case 2 (b), Case 3 (c) and Case 4 (d). Predictions based on B_2 (dashed line) and B_6 (solid line), measurements (o, +).

For a plunging breaker, the wave shape factor continually increases in the surf zone. Here the exponential function $\exp[-40\alpha_B^2\chi_B(1-h/h_B)]$ is used to represent this process. The

function indicates a decrease in shape factor for a spilling breaker after an initial increase, but less effect on a plunging breaker owing to the relatively smaller values of α_B^2 and χ_B .

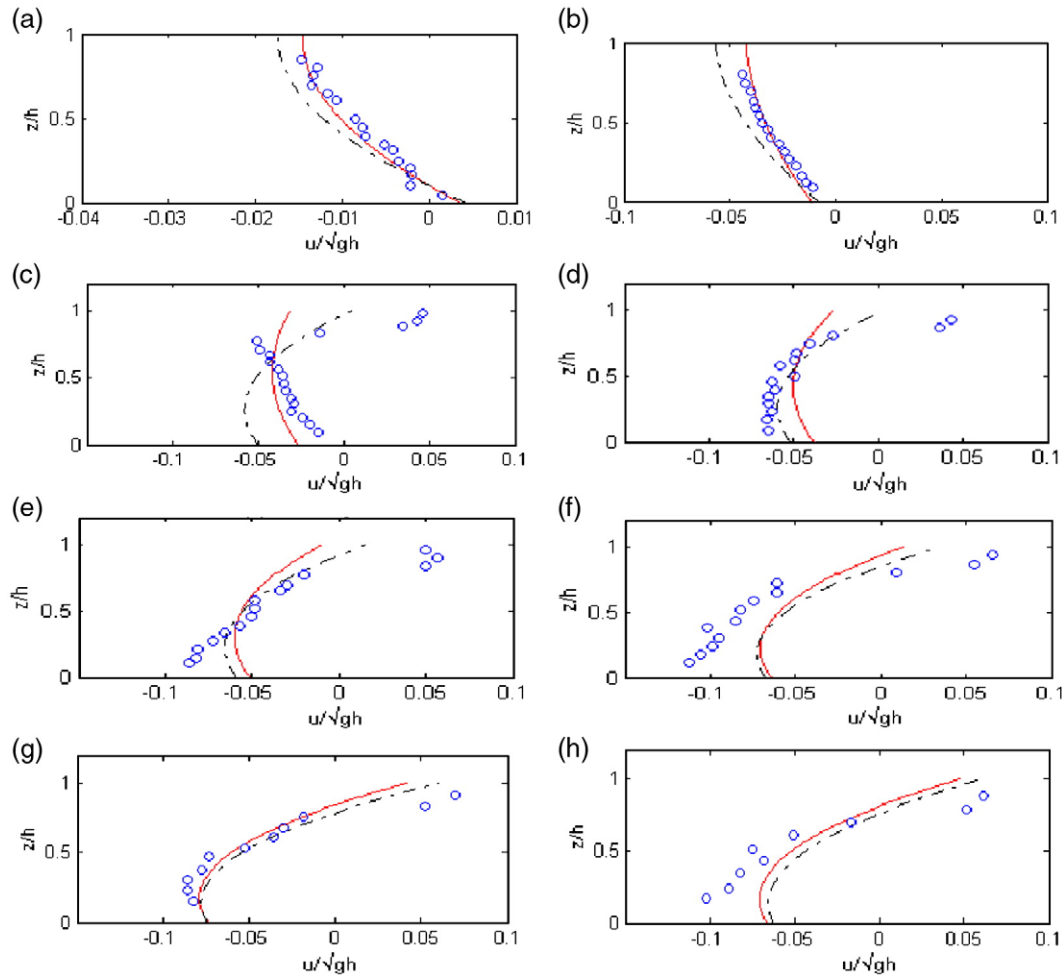


Fig. 19. Current profiles for Case 1. Measurements (o), simulations based on B_2 (dashed line), simulations based on B_6 (solid line).

Inclusion of shape factor value at the breaking point suggests a certain memory in broken waves. Comparisons between the formulations and the simulated data outside and inside the surf zone exhibit a good agreement with the observations. Figs. 14 and 15 illustrate the comparisons for the grouped case $T=5.0$ s, slope=1/50.

4.5.3. Nonlinear phase velocities

For long and high wave waves, permanent wave phase velocity depends on the wave amplitude. The term c^2/gh is not a unit constant, but varies with the wave amplitude. There are several existing theories or formulations to represent nonlinear wave phase velocity. The Stokes theory results from an expansion of the dependent variables based on an assumed small parameter $\epsilon=ka$, where k is the wave number and a is the linear wave amplitude. The solution for Stokes waves is valid in deep or intermediate water depth. In order to mimic the effect of amplitude dispersion in shallow water, Hedges (1976) proposed a simple modification to the linear dispersion relation., which is $c=c_0 \tanh(kh+\epsilon)$. Kirby and Dalrymple (1986) further proposed a composite dispersion relation to model nonlinear effects

over a broad range of water depths. The corresponding wave phase velocity is

$$c = c_0(1 + f_1 \epsilon^2 D) \tanh(kh + f_2 \epsilon) \tag{4.8}$$

where $f_1(kh) = \tanh^5(kh)$, $f_2(kh) = [kh/\sinh(kh)]^4$, $D = \frac{8 + \cosh 4kh - 2 \tanh^2 kh}{8 \sinh^4 kh}$.

The wave number is calculated using linear wave theory in Eq. (4.8). To represent the nonlinear effects in a wide range of water depth, the corrections to Eq. (4.8) are sought here. Instead of using linear wave number, the local wave number determined by the Boussinesq-type model is tried to search for a relationship between wave phase velocity and $\epsilon=ka$. Up to the breaking point, the corrected relation is given as

$$c = c_0(1 - f_1 \epsilon^2 D) \tanh[kh + 0.80f_2 \epsilon]. \tag{4.9}$$

In the surf zone, the observations suggest that wave breaking has some effects on the dispersion relation. Following the initial breaking, the value of ka drops significantly. However, the wave phase velocity does not correspondingly decrease greatly.

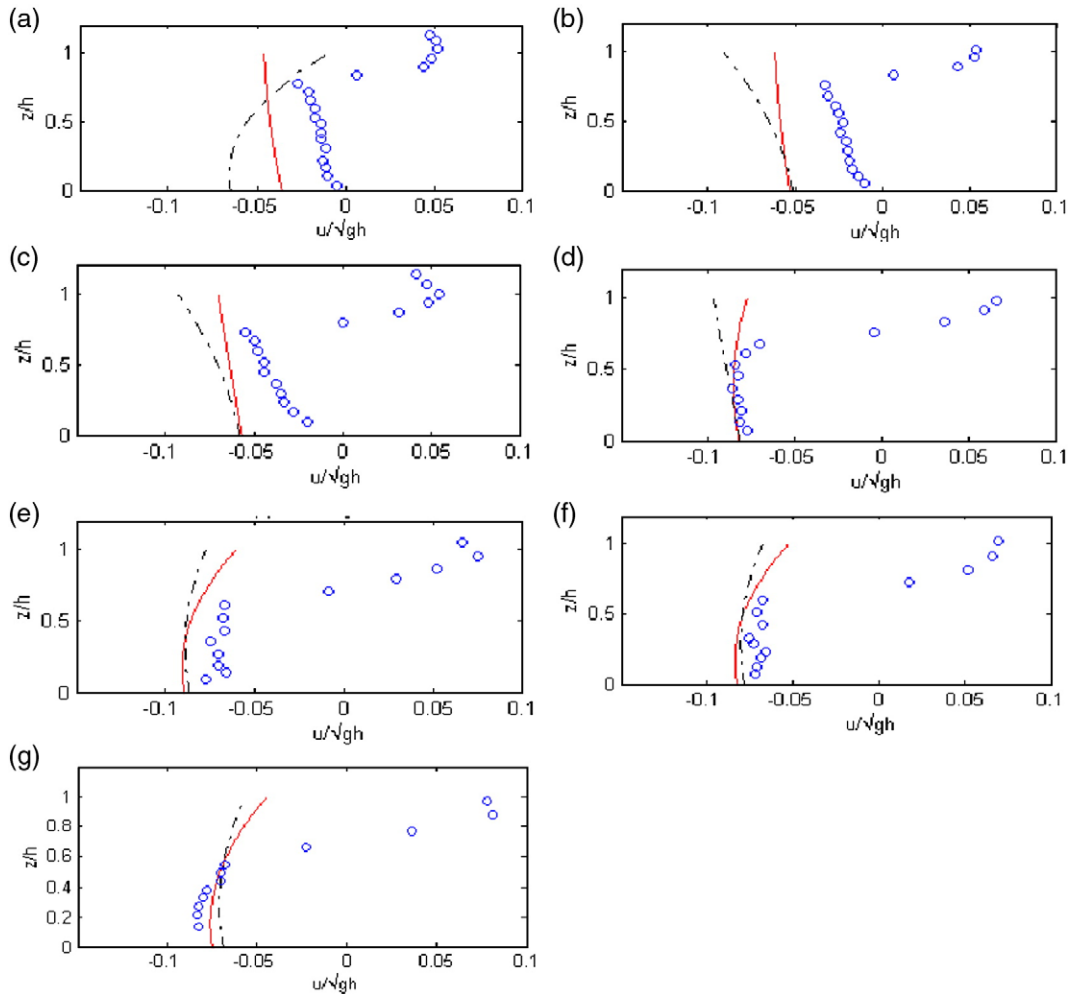


Fig. 20. Current profiles for Case 2. Measurements (o), simulations based on B_2 (dashed line), simulations based on B_6 (solid line).

It is found that wave phase velocity can be corrected by the change of local wave steepness H/L and relative location in the surf zone. This leads to

$$c = \psi c_0 (1 + f_1 \varepsilon^2 D) \tanh[kh + 0.80 f_2 \varepsilon] \quad (4.10)$$

where $\psi = 1 + (h/h_B)^{0.8} (s_p/s - 1)$, $s = H/L$, $s_p = H_p/L_p$.

Fig. 16 demonstrates the results of numerical observations and analytical solutions from Eqs. (4.9) and (4.10). The comparisons suggest a good agreement in a wide range of the nearshore region.

5. Application of the new formulations

The formulations of nonlinear wave properties have been completed based on the very extensive numerical simulations. The nonlinear corrections of shape factor, shoaling coefficient and phase velocity are given in their relationships with the local wave parameters, such as Irribarren number, Ursell number and wave steepness. In other words, the proposed relationships allow the more representative shape factor, phase velocity and wave height to be corrected directly from the local wave parameters.

To apply the new formulations, they are incorporated into the SHORECIRC model. The desired nonlinearities are approached using the iteration technique based on the new formulations. Because the nonlinear expressions are formulated in terms of the local wave parameters, the initial values can be the results

from either the linear wave theory or the weakly nonlinear wave theory.

Cases 1, 2, 3, and 4 introduced in Section 4.3 are used to compare with the numerical simulations. These experimental data involve various bathymetries and incident wave conditions with extensive measurements of mean water levels and currents. The numerical flumes are built with the same dimensions as those original physical experiments.

In the original SHORECIRC model, the wave field is calculated using Kirby and Dalrymple (1986) which is based on the weakly nonlinear theory. The radiation stress and volume flux are estimated by either a linear shape factor 0.125 or a reduced value to correct the nonlinear effect. The approaches have been proved to be far from satisfactory, see Svendsen (1984) and Svendsen and Putrevu (1993). Case studies show that they can overestimate the set-up and currents up to 40%–100%.

A series of simulation results using the newly formulated equations are illustrated in Figs. 17–22. The locations of current profile can be found in the corresponding papers, i.e. Ting and Kirby (1995, 1996, 1994), Govender et al. (2002) and De Serio and Mossa (2006).

The comparisons suggest the predictions of set-up from the sixth-order formulation are closer to the measurements than those using the second-order formulation. The average differences of maximum set-up between simulations and measurements are less than 15%, which can be regarded as a significant improvement. For the current profiles, the improvements from the second and sixth-order formulations are inconsistent. Some locations show a marginal change; this suggests that the current profiles would require more than just the correct wave shape. More physical processes are needed to determine the current profiles, such as the momentum transfer between the surface roller and the underlying water, and the mixing of momentum over the water column. The other possible reason may be the result of new expressions that are statistically formulated and are not able to exactly represent one specific case.

6. Conclusions

In this work, the nonlinear wave properties, radiation stress and volume flux, are investigated. The studies presented here are based on new theoretical development, advancement of a numerical simulation and comparison with experimental data. The importance of wave nonlinearity has been clearly demonstrated to understand the characteristics of currents and variation of mean water level.

In the modelling efforts, the integrated wave properties are specially targeted. Novel mathematical formulations of radiation stress and volume flux for shallow water waves are derived. The formulations include the higher-order surface elevations up to the sixth-order, which were neglected in previous studies. To quantitatively describe these properties, a comprehensive investigation of the wave fully nonlinear transformation on a beach has been conducted in a numerical flume using the COULWAVE model. Based on the results of the numerical simulations, the expressions of the wave shoaling coefficient (Eq. (4.1)), the

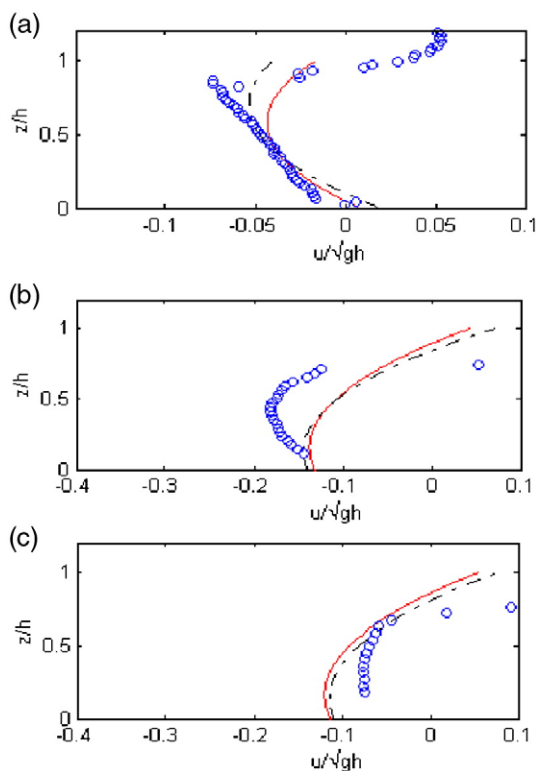


Fig. 21. Current profiles for Case 3. Measurements (o), simulations based on B_2 (dashed line), simulations based on B_6 (solid line).

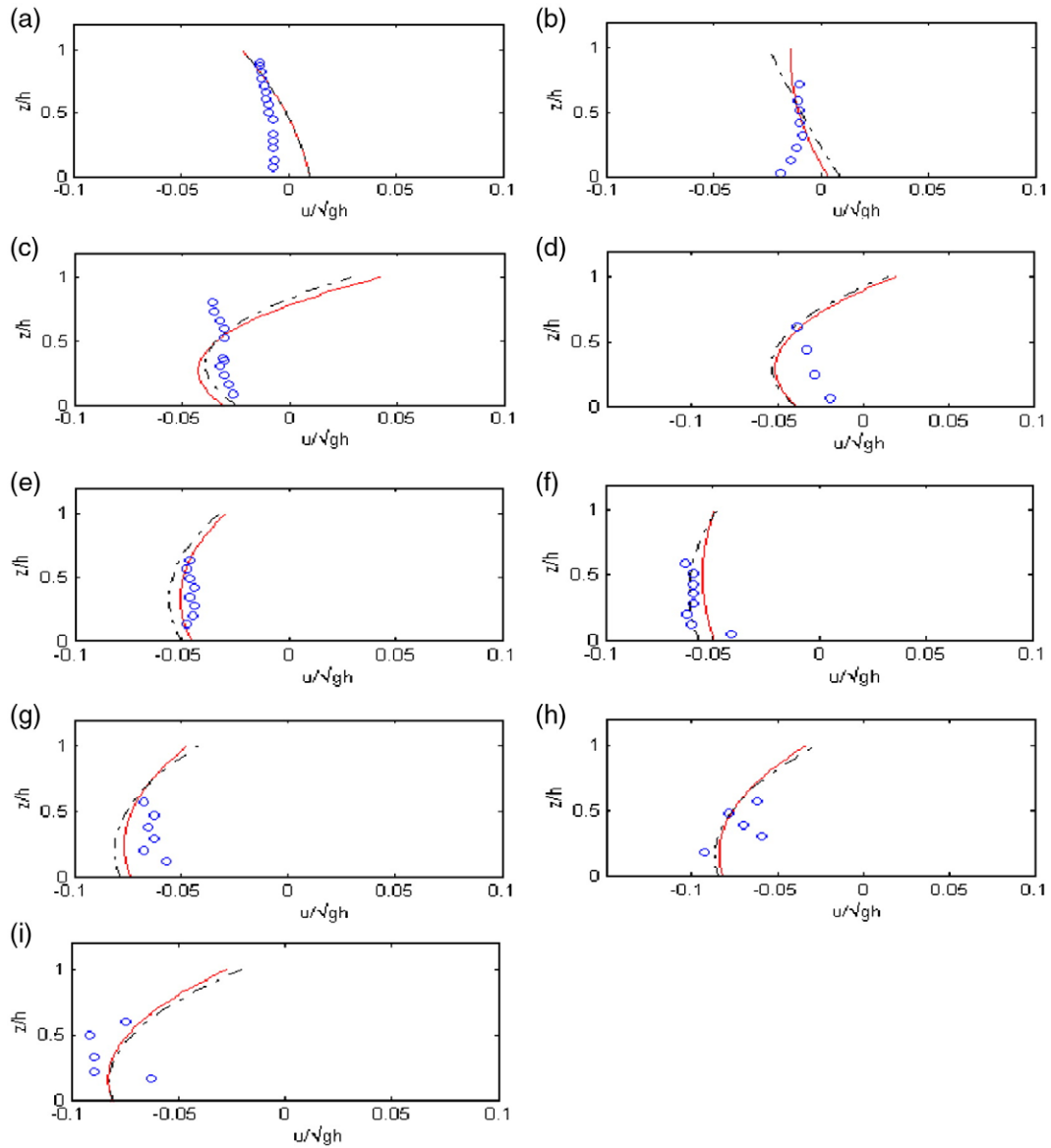


Fig. 22. Current profiles for Case 4. Measurements (o), simulations based on B_2 (dashed line), simulations based on B_6 (solid line).

second-order and the sixth-order shape factors (Eqs. (4.2)–(4.7)) and the phase velocity (Eqs. (4.9) and (4.10)) have been formulated.

The second-order and the sixth-order shape factors exhibit the same variation trend, but differ in their magnitudes. The sixth-order shape factors (B_6) give a lower value than the second-order (B_2). At the breaking point, the wave shape factors present the lowest value, and the shape factor can be as low as 0.025 (B_2) and 0.23 (B_6), much smaller than a sinusoidal wave. For all simulated cases B_2 is 5–23% bigger than B_6 at the breaking point.

Two important features have been identified from the research. The shape factors are reduced as the Ursell numbers increase. However, the decrease of shape factor becomes slow after the Ursell number is larger than 1500. It is also found that the traditional interpretation of wave shape factor corresponding only on the local Ursell number is inadequate. Another parameter, the Irribarren number, plays an important role in deter-

mining the shape factors as well. When the Irribarren numbers increase, the shape factors tend to increase. In the surf zone, the shape factor is well controlled by the local wave steepness, shape factor at the breaking point and the location in the surf zone.

The shoaling coefficients were investigated by comparison of the linear shoaling coefficients and the fully nonlinear shoaling coefficients simulated by the COULWAVE model. The results demonstrate that their ratio has a strong connection to the local Ursell numbers. Regarding the phase velocity, the dispersion relations representing the nonlinear effects have been sought in a wide range of water depth. In the present work, the formulations are derived by a modification to the equation proposed by Kirby and Dalrymple (1986).

The applications of the new formulation suggest that, by inclusion of the nonlinear formulations in the basic hydrodynamic model, the predictions of mean water level have been improved. The sixth-order formulation of shape factor produces

a better estimation than the second-order formulation. The improvements on current profile are marginal at some locations. It implies that, in addition to the radiation stress and volume flux, the current profiles are determined by more physical process.

Acknowledgments

The authors would extend sincere thanks to Dr. Francis C. K., Ting, in the South Dakota State University, USA, and Dr. K. Govender in the University of Durban-Westville, South Africa for generously providing their experimental data which are used in the research.

References

- De Serio, F., Mossa, M., 2006. Experimental study on the hydrodynamics of regular breaking waves. *Coastal Engineering* 53, 99–113.
- Dean, R.G., Dalrymple, R.A., 1991. *Water Wave Mechanics for Engineers and Scientists*. World Scientific.
- Ebersole, B., Dalrymple, R.A., 1980. Numerical modeling of nearshore circulation. *Proc. 17th Int. Conf. Coastal Engineering*.
- Goda, Y., 2000. *Random Seas and Design of Maritime Structures*. World Scientific Publishing Co. Pet. Ltd.
- Govender, K., Mocker, G.P., Alport, M.J., 2002. Video-imaged surf zone wave and roller structures and flow fields. *Journal of Geophysical Research* 107 (NO. 0).
- Hansen, J.B., 1990. Periodic waves in the surf zone: analysis of experimental data. *Coastal Engineering* 14, 19–41.
- Hedges, T.S., 1976. An empirical modification to linear wave theory. *Proceedings of the Institution of Civil Engineers* 61, 575–579.
- Kirby, J.T., Dalrymple, W.R., 1986. An approximate model for nonlinear dissipation in monochromatic wave propagation models. *Coastal Engineering* 9 (No. 6), 545–561.
- Longuet-Higgins, M.S., Stewart, R.W., 1960. Changes in the form of short gravity waves on long waves and tidal currents. *Journal of Fluid Mechanics* 8, 565–583.
- Longuet-Higgins, M.S., Stewart, R.W., 1962. Radiation stress and mass transport in gravity waves with application to 'surf beats'. *Journal of Fluid Mechanics* 13, 481–504.
- Longuet-Higgins, M.S., Stewart, R.W., 1964. Radiation stresses in water waves; a physical discussion with applications. *Deep-Sea Research* 11, 529–562.
- Lynett, P., 2006. Nearshore modelling using high-order Boussinesq equations. *Journal of Waterway, Port, Coastal, and Ocean Engineering* 132 (5), 348–357 (ASCE).
- Lynett, P., Liu, P.L.-F., 2004. A two-layer approach to water wave modeling. *Proceedings of the Royal Society of London. A* 460, 2637–2669.
- Otta, A.K., Schäffer, H.A., 1999. Finite-amplitude analysis of some Boussinesq-type equations. *Coastal Engineering* 36, 323–341.
- Peregrine, D.H., 1983. Breaking waves on beaches. *Annual Review of Fluid Mechanics* 15, 149–178.
- SPM, 1984. *Shore Protection Manual*. U.S. Army Corps of Engineers, Waterways Experiment Station, Vicksburg, MS.
- Svendsen, I.A., 1984. Wave height and set-up in a surfzone. *Coastal Engineering* 8 (4), 303–330.
- Svendsen, I.A., 2006. *Introduction to Nearshore Hydrodynamics*. World Scientific.
- Svendsen, I.A., Staub, C., 1981. Horizontal particle velocity in long waves. *Geophysical Research* 86, 4138–4148.
- Svendsen, I.A., Putrevu, U., 1993. Surf zone wave parameters from experimental data. *Coastal Engineering* 19, 283–310.
- Svendsen, I.A., Putrevu, U., 1995. Surf-zone hydrodynamics. *Advances in Coastal and Ocean Engineering*. World Scientific, pp. 1–78.
- Svendsen, I.A., Qin, W., Eberlose, B.A., 2003. Modelling waves and currents at the LSTF and other laboratory facilities. *Coastal Engineering* 50, 19–45.
- Svendsen, I.A., Haas, K. and Zhao, Q., Version 2.0. Quasi-3D nearshore circulation model SHORECIRC, Centre for Applied Coastal Research, University of Delaware.
- Ting, F.C.K., Kirby, J.T., 1994. Observation of undertow and turbulence in a laboratory surf zone. *Coastal Engineering* 24, 51–80.
- Ting, F.C.K., Kirby, J.T., 1995. Dynamics of surf-zone turbulence in a strong plunging breaker. *Coastal Engineering* 24, 177–204.
- Ting, F.C.K., Kirby, J.T., 1996. Dynamics of surf-zone turbulence in a spilling breaker. *Coastal Engineering* 27, 131–160.
- Van Dongeren, A.R., Svendsen, I.A., 1997. *Quasi 3-D Modeling of Nearshore Hydrodynamics*. University of Delaware.
- Wei, G.E., Kirby, J.T., Grilli, S.T., Subramanya, R., 1995. A fully nonlinear Boussinesq model for surface waves: part 1. Highly nonlinear unsteady waves. *Journal of Fluid Mechanics* 294, 71–92.
- Wu, C.-S., Liu, P.L.-F., 1985. Finite element modeling of nonlinear coastal currents. *Journal of Waterway, Port, Coastal and Ocean Engineering* 111 (no.2), 417–432.